Intraband transitions in quantum dot–superlattice heterostructures

F. F. Schrey,* L. Rebohle,† T. Müller, G. Strasser, and K. Unterrainer
Photonik Institut und Institut für Festkörperelektronik, Technische Univerität Wien, Floragasse 7, A-1040 Wien, Austria

D. P. Nguyen,‡ N. Regnault, R. Ferreira, and G. Bastard
Laboratoire Pierre Agrain—Ecole Normale Supérieure, 24 rue Lhomond, F-75005 Paris, France

(Received 16 June 2005; published 13 October 2005)

We present a scheme of adjusting the mid-infrared absorption properties to desired energy transitions in quantum dot-based photodetectors by combining band gap engineering with the self-organized growth of quantum dots. Embedding the self-organized InAs quantum dots into an AlAs/GaAs superlattice enables us to tune the optical transition energy by changing the superlattice period as well as by changing the growth conditions of the dots. Using a one-band envelope function framework, we are able, in a three-dimensional calculation, to predict the absorption spectra of these devices as well as their polarization properties. These calculations further predict a strong impact of the dots on the superlattice minibands. By comparing aligned, periodic dot stacks with nonperiodic dot arrangements within the superlattice, we can experimentally confirm this prediction.

DOI: 10.1103/PhysRevB.72.155310 PACS number(s): 85.35.Be, 85.60.Gz, 73.21.Cd, 78.67.Hc

I. INTRODUCTION

Self-assembled quantum dots gain more and more importance as functional elements within semiconductor devices. Especially GaAs/AlAs superlattice (SL) systems with embedded InAs quantum dots (QD) initiated considerable research activities[1–14] in recent years. Due to their electronic structure in the conduction band, InAs QDs are sensitive to optical fields and cover energetically the important spectral region between 30 and 400 meV.[1–9,15,16] Thus, dot devices are predestined to be used as mid- and far-infrared (MIR/FIR) photodetectors. In contrast to purely quantum well-(QW-) based detectors with their vanishing sensitivity under normal incidence geometries, QD devices offer more promising polarization selection rules[17–19] for detector applications. Furthermore, one would expect better noise properties from QD devices because of their discrete energetic structure, which drastically reduces unwanted electron scattering mechanisms.[20,21]

However, it cannot be ignored that SL structures offer a very convenient way of designing transition energies by band structure engineering. For QDs, the optical transitions can rather be tuned than designed: For example, a careful choice of the growth conditions influences the dot size[10] and thus the intradot energy scheme. Further, changes of the QD environment like inserting an AlAs layer close to the dot[11] or the replacement of the surrounding GaAs matrix by $Al_xGa_{1-x}As$ influence the conduction band offset between the dot and this matrix.[12,22] Although these procedures allow obtaining dot ensembles with transitions in the desired energy range between 30 and 400 meV, they cannot overcome inhomogeneous broadening effects resulting from size distribution in the self-assembly of the QDs.

In this paper we will show that embedding of InAs QDs into AlAs/GaAs SL structures can overcome most of the deficiencies of each system alone and combine the advantages of both structures. In addition to the experimental investigation of different QD-SL combinations, we develop a model that allows predicting the absorption and polarization properties of these QD infrared photodetectors (QDIP) for given dot sizes and SL periods. Comparing the model and experiment, we can show that the small ratio between dot height and lateral dot size and the SL-induced conduction band quantization are the dominant parameters that influence the MIR and FIR photoresponse associated with the photon absorption from the bound QD ground state to the QD continuum states.

II. DEVICES

All investigated samples are grown by molecular beam epitaxy (MBE) on smoothed semi-insulating (001) GaAs substrates. The 650 nm thick, Si-doped GaAs back-contact layer, grown at 600 °C, is followed by the SL/QD structure, whereby the dots are grown in the Stranski-Krastanov mode by depositing two monolayers of InAs. All layers above the back-contact are grown at 485 °C to avoid intermixing between barriers, wells, and dots. The parameters are chosen to obtain a lateral dot density of about 5×10^{10} dots/cm^2 per layer, controlled by atomic force microscopy measurements.[23] For the application as photodetectors, the dots are modulation doped with one electron per QD. The samples differ in the number of QD layers, their vertical layer spacing or their SL period. Table I gives an overview over the investigated samples, which are sketched in Fig. 1.

The samples can be divided into two subsets: The first set contains the so-called multiple dot (MD) structures, i.e., the

TABLE I. Devices.

Device	MD-A	MD-B	MD-C	DD	SD
SL period L (nm)	10	11	14	11	11
Number of QD layers	30	20	20	20	20
Number of AlAs barriers	—	20	20	40	60

 ©2005 The American Physical Society

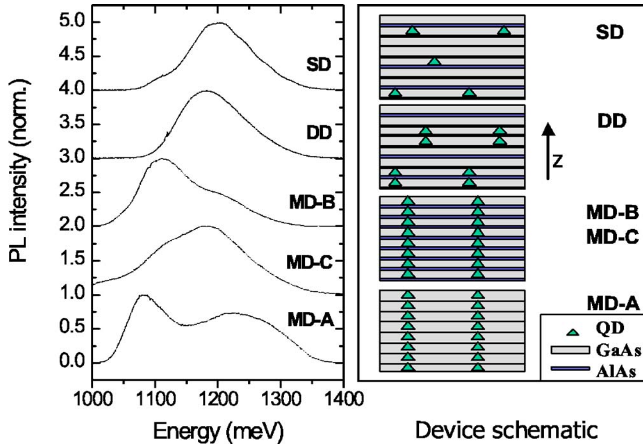

FIG. 1. (Color online) Interband photoluminescence spectra of the investigated devices. On the right: Sketches of the different device layouts. The arrow denotes z, the growth direction.

vertical spacing between subsequent dot layers is chosen small enough to guarantee vertical alignment (stacking) of the QDs due to strain minimization.[5] The second set contains vertical single dot (SD) and vertical double dot (DD) devices. They are used as control samples for the MD devices to study the influence of the vertical periodicity of the QDs on the AlAs/GaAs SL. Depending on their performance as QDIPs, they will further allow us to estimate experimentally how far QDs and a surrounding SL can be regarded as independent systems.

We use photoluminescence (PL) spectroscopy with excitation at 632.8 nm to characterize the samples as shown in Fig. 1 at a temperature of 5 K. The PL spectra show a similar behavior within each subset with ground state transitions at about 1100 and 1200 meV, respectively. In order to perform photocurrent (PC) and current-voltage (IV) measurements, the samples are processed by photolithography, wet chemical etching, and several polishing steps into QDIPs.[6] Their electrical contacts consist of thermally alloyed Ni/Ge/Au layers. All experiments are carried out at 5 K in optical helium flow cryostats. The IV characteristics are recorded with a HP 4155A SC parameter analyzer while the spectral and polarization dependence of the photoresponse of the QDIPs is measured with a FTIR spectrometer and a thermal infrared source. The PC signal is read out by a Lock-In amplifier while the excitation is modulated with a mechanical chopper.

III. MODEL

Very detailed predictions about the energetic structure of InAs QDs have been made by Stier *et al.*,[24] in the framework of multiband *kp* theory or by Williamson and Zunger,[25] Zunger *et al.*[26] and Lee *et al.*[27] by using accurate atomistic approaches. While their approaches mostly focus on the understanding of the properties of bound states within the QD, we choose a simpler one-band envelope function framework in order to investigate the extended continuum states of the dots and their converse influence on a surrounding SL. Especially, we focus on the optical properties of the bound-to-bound transitions within the QD and the bound-to-continuum transitions from the QD into the surrounding GaAs matrix or the AlAs/GaAs SL.

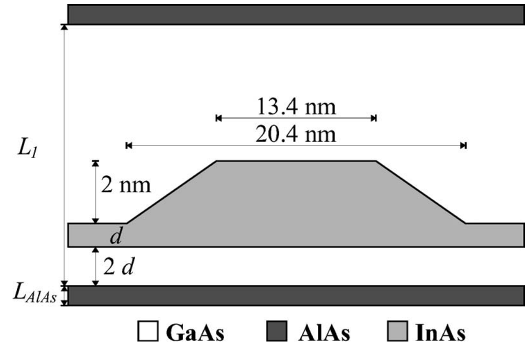

FIG. 2. Schematic representation of the supercell including the dot and its WL. $L_1=10$ nm (MD-A, MD-B) or 13 nm (MD-C) and $L_{\mathrm{AlAs}}=0$ (MD-A) or 1 nm (MD-B, MD-C).

Because overgrown InAs QDs within a GaAs matrix exhibit a flat, lenslike shape[28] with a typical aspect ratio (height to base radius) h/R of 2–3 nm/10 nm we can use a geometric simplification of the QD by modeling them as truncated cones.[29–31] Despite this simplification our method has been proven to be successful in quantitatively predicting anticrossings associated with polarons in bound-to-bound magneto-optical transitions of InAs/GaAs QDs.[30,31]

In our model the effective Hamiltonian is[32]

$$H = H_0 + \delta V = \frac{p^2}{2m^*} + V(\rho,z) + \delta V(r), \tag{1}$$

where m^* is the (constant) effective electron mass (here $0.07\ m_0$)[30], $V(\rho,z)$ is the isotropic part of the potential energy, $\delta V(r)$ is that part of the potential energy, which does not display cylindrical symmetry (as, e.g., caused by a shape anisotropy[33] like an elliptical basis instead of a circular one[30] or as arising from piezoelectric fields[24]). The eigenstates of H_0 are eigenfunctions of the angular momentum L_z with eigenvalues l; i.e., the states will be denoted as $S, P_+, P_-, \ldots$. With a conduction band (CB) discontinuity between InAs and GaAs of 0.4 eV[25] and the truncated cone approximation of the dot with a lower (upper) radius of 10.2 nm (6.7 nm) and a height of 2 nm on an InAs wetting layer (WL) of thickness $d=0.565$ nm, as depicted in Fig. 2 we obtain a value of about 50 meV for the lowest bound-to-bound $(S \rightarrow P_\pm)$ transition and 160 meV from the lowest bound state to the onset of the GaAs continuum. The latter value is mostly determined by the vertical dot dimension, while the former is governed by the lateral QD size.

As explained above, most of the investigated QDIPs use vertically stacked dot planes with a short period L to increase the infrared absorption. This offers the possibility to search for Bloch-like solutions of H:

$$\psi_{k_z}(x,y,z+L) = e^{ik_zL}\psi_{k_z}(x,y,z). \tag{2}$$

Thus, the stacking of dots and the insertion of AlAs barriers effectively structures the QD's continuum and the eigenenergies of H become periodic functions of k_z. We have to mention here that we exclude with this ansatz the SD and DD

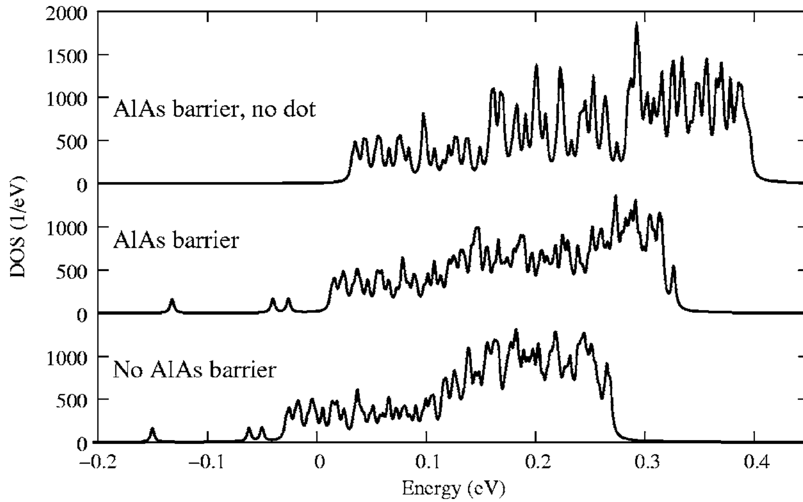

FIG. 3. Density of states of even-even symmetry (even wave function in x and y) for an electron with $L=12$ nm (for $k_z=0$). The energy zero is taken at the onset of the GaAs conduction band edge.

devices from our model since these structures do not allow solutions of the form shown in Eq. (2), because the vertical periodicity is missing.

In the following we calculate the transition energies and polarizations for infrared absorption of a QD within a cylindrical supercell with 200 nm radius and a length of $L=L_1+L_{\mathrm{AlAs}}$ along the growth direction z as sketched in Fig. 2, with band offsets of 1.08 eV for AlAs/GaAs[34] and 0.4 eV for InAs/GaAs.[25] This Bloch-like ansatz requires the wave functions to vanish at the lateral boundaries and to be periodic at the vertical boundaries; i.e., the vertical periodicity mimics the QD stack and the SL automatically. Thus, the length L of the supercell becomes the SL period. Numerically we perform a block diagonalization of the dot Hamiltonian on a large basis of 10 000 functions[35] with an elementary cubic cell size of $d=0.565$ nm. It is a Bessel basis for the radial motion:

$$\psi_{lnq}(\vec{r}) = C_{lnq} \cdot \exp(il\theta) \cdot J_l\left(\lambda_n^l \frac{r}{R}\right) \cdot \exp\left(i\frac{2\pi qz}{L}\right), \quad (3)$$

where C_{lnq} is a normalization constant, l the angular quantum number, q an integer, and λ_n^l are zeros of the first kind Bessel function J_l. The first 200 eigenstates are evaluated by exactly diagonalizing H with the Lànczos algorithm,[36] while taking into account contributions from the first Brillouin zone $k_z \in]-\pi/L, \pi/L]$ as well.

At first, we calculate the density of states (DOS), using a symmetrized plane wave basis, at $k_z=0$ for different devices with and without dots or AlAs barriers, as depicted in Fig. 3. Without loss of generality we show for better clarity only the DOS of even-even symmetry, i.e., even wave functions in the x and y directions. The energy origin in this figure is taken at the conduction band edge of GaAs. In case of the pure AlAs/GaAs SL (upper curve) we observe a blueshift of the "continuum" onset 16 meV above the bulk GaAs CB, which corresponds to the first miniband of a SL in typical one-dimensional SL calculations.[37] In the following we denote the continuum region of the AlAs/GaAs SLs as a quasicontinuum in order to underline the presence of minibands. The shape of the DOS in the quasicontinuum region resembles roughly the well-known step function for the DOS of a QW SL (k_z is fixed). The sharp peaks in the quasicontinuum region are caused by the discrete nature of the eigenfunctions and the limitation to the first 200 eigenfunctions. This limitation causes additionally the unphysical, high-energy cutoffs in Fig. 3. For the case of a QD stack in a GaAs matrix (lower curve), we see three sharply peaked bound states below the GaAs CB and a redshifted onset of the continuum at −15 meV. The three lowest peaks correspond to the QD's S-like ground state and its excited S- and D-like states. The onset of the quasicontinuum can be identified with the wetting layer (WL) of the dot. Note that in this periodic arrangement the WL forms a SL by itself (also with period L) and thus differs from a WL for diluted dots in GaAs. In the second case (middle curve) the dots are combined with the AlAs/GaAs SL. This results in a redshift for the minibands as compared to the first case and into a blueshift for the QDs as compared to the third case (lower curve). Thus, the QD represents a deep attractive perturbation for the carriers in AlAs/GaAs/InAs SL, and *vice versa* the energy scheme of the InAs QD's continuum is considerably restructured by the SL.

In our next step, we calculate the absorption coefficient $\alpha(\omega)$ of the devices denoted as MD-A, MD-B, and MD-C, according to

$$\alpha(\omega) \propto \sum_n |\langle s|E \cdot r|n\rangle|^2 \delta(\varepsilon_n - \varepsilon_s - \omega), \quad (4)$$

where n labels the discrete continuum states, ε_n the corresponding energies, and E the light polarization. Comparing $\alpha(\omega)$ for different polarizations of the light (Figs. 4–6), a pronounced anisotropy of the optical absorption becomes visible: For in-plane ($E \perp z$) polarizations, the so-called normal incidence, TE or s polarization, the strongest absorption in Fig. 4 is caused by the bound-to-bound transitions while the bound-to-continuum absorption is nearly three orders of magnitude smaller. The bound-to-bound transition ($S \rightarrow P_\pm$) exhausts almost all the oscillator strength (OS) for transitions within these devices and nearly saturates the Thomas-Kuhn-Reich sum rule. This implies already a weakened absorption for all other transitions and polarizations since the OS sums up to one in a given polarization for all transitions. Taking

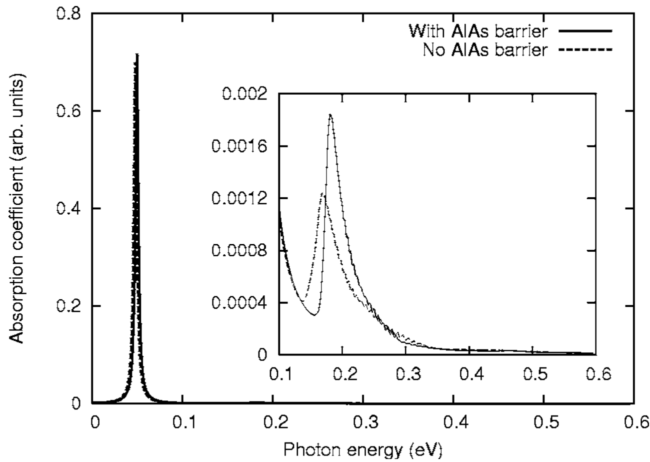

FIG. 4. Absorption coefficient for in-plane polarization with $L_1=10$ nm (MD-A and MD-B). The inset shows a zoom of the bound-to-continuum absorption.

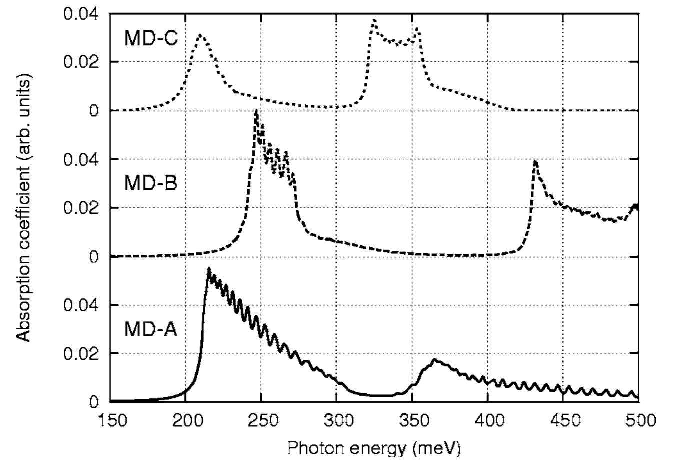

FIG. 6. Absorption coefficient for a z-oriented polarization. Full line: $L=10$ nm (MD-A). Dashed line: $L=11$ nm (MD-B). Dotted line: $L=14$ nm (MD-C). The same scale for the vertical axis is used for the three samples (the same arb. units as in the inset of Fig. 4).

into account a slight ellipticity of the dot ($R_y/R_x=0.9$), the main absorption under normal incidence further splits into a strongly x- or y-polarized doublet, as depicted in Fig. 5. Thus, the shape anisotropy causes additionally an energy difference between the x and y transition, which might even be visible in the PC signal, as we will see later in the experimental part of this publication.

Absorption spectra for polarizations parallel to the growth axis z (TM or p polarization) are shown in Fig. 6 for all MD devices: Strikingly, there is no absorption corresponding to a bound-to-bound transition of the QD, but the absorption for bound-to-continuum transitions is quite strong. Both effects can be understood by regarding the localization of the wave functions within the supercell more closely: Because of the small dot height in the growth direction, the virtual bound states (or resonances) for the z motion will be found energetically high above the InAs edge. Simultaneously, the periodicity of the whole structure in z gives rise to an energy spectrum periodic in k_z with eigenfunctions fulfilling [Eq. (2)] and localized roughly in the same region where the virtual bound states of the dot are situated. A comparison to a separable model[32,38] then evidences that the QD ground state couples preferentially with continuum states that have nearly the same lateral extension, i.e., all other continuum states as well as the excited QD bound states, have no significant overlap with the ground state for p polarization. Note that it is the vertical periodic arrangement of the QDs that introduces this polarization selection rule for bound-to-continuum transitions, not the AlAs/GaAs SL.

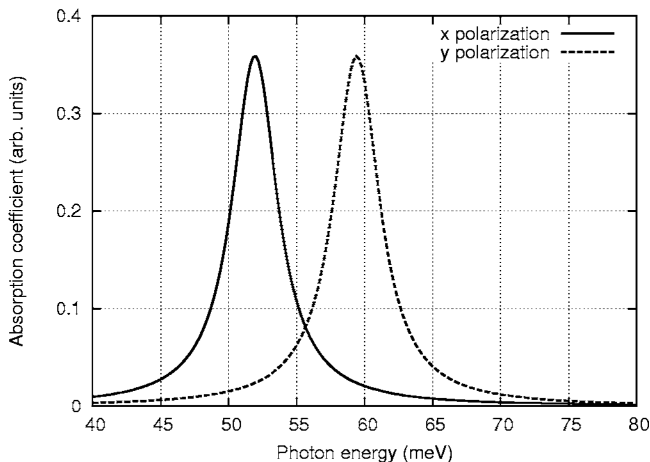

FIG. 5. Absorption coefficients for x- and y-oriented polarizations with $L_1=10$ nm (MD-B), AlAs barrier, and a slightly elliptical dot ($R_y/R_x=0.9$).

Further, it should be noted that the absorption spectra in Fig. 6 reflect the presence of minibands with corresponding widths of $\Delta E_2=E_2(k_z=0)-E_2(k_z=\pi/L)\approx 25$ (40) meV and $\Delta E_3\approx 50$ (80) meV for the device MD-C (MD-B). The sawtooth structure on the absorption peaks is a numerical artifact resulting from the summation over a limited number (about 50) of k_z values within the first Brillouin zone and has no physical meaning.

In summary, we emphasize that the QD continuum states inserted into a SL cannot be considered as the result of a small perturbation of one system (e.g., the SL) by the other (the QDs and its WL). In this periodic arrangement the presence of the QDs changes the position of the SL minibands significantly and imposes a polarization dependence of the bound-to-continuum transition while the SL restructures the QD continuum and shifts the QD bound states to slightly higher energies. Thus, the combination of both systems, dots and QWs, does not allow an independent design of each subsystem.

For the application as photodetectors, the stacking of the QDs causes a disadvantageous polarization dependence (p-pol.) for bound-to-continuum transitions, which are normally preferred for MIR detectors. However, the strong OS for the bound-to-bound transitions suggests a combination of both systems in a way that the bound excited states of the dots are energetically pushed into the dot/SL continuum, e.g., by reducing the dot size or by rapid thermal annealing.[10] Such a device should exhibit a strong absorption under normal incidence related to a strong photocurrent extracted via the SL minibands. On the other hand, we can guess from the

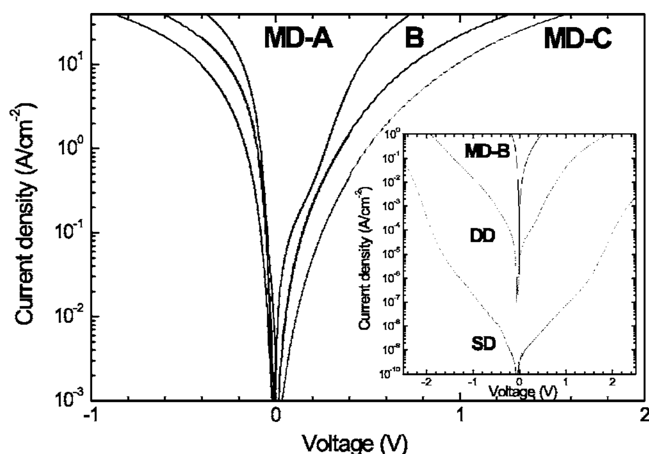

FIG. 7. Current-voltage (IV) characteristics of devices MD-A, MD-B, and MD-C (inset: MD-B, DD, SD). All devices show an asymmetric diodelike behavior. The IV shape changes drastically between MD, DD, and SD devices.

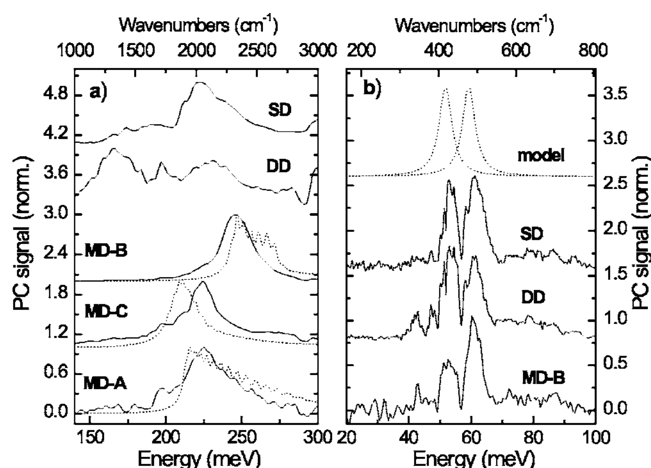

FIG. 8. (a) Photocurrent spectra in the mid-infrared region. (b) Far-infrared spectra: The double peak structure is attributed to the shape asymmetry of the QDs. For a comparison, the calculated spectra are plotted as dotted lines.

periodic model a possible behavior of our SD and DD devices. In these detectors, we still have the periodicity of the AlAs/GaAs SL, but the dots represent now a large perturbation of the minibands within some of the SL periods. This perturbation should disturb the electron transport through the SL and a strong decrease of the photocurrents is expected.

IV. EXPERIMENTAL RESULTS

As mentioned above, the PL ground state emission of the investigated samples in Fig. 1 amounts to 1100 meV for the MD devices and to about 1200 meV for SD and DD. Since both subsets are grown under the same conditions, we suppose that the difference of the PL onset is caused by different strain conditions for the dots due to their vertical alignment: The vertical alignment of the QDs is driven by the minimization of the free energy of the dots and the corresponding WL. Thus, the free energy, expressed mainly by the strain of the dots,[39] will be lower for QDs in MD devices than in the SD and DD case. Consequently, the ground state emission of the MD devices is redshifted toward the SD/DD devices. The slight energetic deviation of MD-A compared to the other, blueshifted MD devices can either be caused by a small deviation in the MBE growth parameters or it can be interpreted as the mutual influence of the SL onto the bound QD states, as discussed in Sec. III and Fig. 3. In all samples, the QD size distribution causes a spectral broadening of the peaks of at least 40 meV and a spectral overlap between ground and excited states.

Figure 7 shows the IV characteristics of the QDIPs at a temperature of 4.2 K. As expected, all devices exhibit an asymmetric diodelike behavior. Adding AlAs barriers into the structure the dark current decreases by more than one order of magnitude in descending order of MD-A, MD-B, and MD-C. In contrast to MD-A the electrons in MD-B have to tunnel additionally through the AlAs barriers of the AlAs/GaAs/InAs SL. Further, the width of the minibands as well as their energetic positions decrease in the order of MD-A, MD-B, and MD-C, i.e., electrons in MD-C have to tunnel through a higher barrier than in MD-B.

In case of the SD and DD devices (the inset of Fig. 7), the dark currents drop drastically by several orders of magnitude. We attribute this to the strong influence of the dots on the electronic transport within the SL. If we break the strict periodicity of the combined QD-SL system, we obtain a system in which a rather normal one-dimensional SL with its typical energetic properties is directly attached to a very short QD-SL system. Thus, we will have a vertical misalignment of the quasicontinuum states, i.e., the minibands. As we will see below this reduces not only the unwanted dark currents, but also the desired photocurrents drastically.

The unpolarized and unbiased PC spectra of the MD devices shown in Fig. 8(a) are characterized by a single, roughly 40 meV broad main peak around 225 meV for MD-A and MD-C and around 247 meV for MD-B. These values are in good agreement with the calculated spectra from Fig. 6 (plotted as dotted lines in Fig. 8 for a better comparison). Thus the recorded PC spectrum can be interpreted as ionization of the electrons from the bound QD ground states into the quasicontinuum of the combined QD-SL structure. In this context, the broadening of the PC peaks is caused by the size distribution of the QDs and their corresponding bound states, as well as by the width of the minibands. The latter effect is also in very good agreement with our model, where the width of the first absorption peak decreases in the order of MD-A, MD-B, and MD-C. The smoothness and the high signal to noise ratio (SNR) of the main absorption peaks of the MD devices can be attributed to the decreased dark currents due to the insertion of AlAs QWs and to a homogenization of the QD size distribution within each QD stack due to the vertical alignment of the dots and the corresponding strain minimization.

Without periodic, vertical alignment of the QDs, the PC spectrum becomes more complex for the SD and DD detectors: Several PC peaks in the energy range between 170 and 320 meV with a comparatively small SNR can be observed. Despite that we cannot calculate the spectra for the SD and

DD devices, because their broken symmetry violates the Bloch theorem [Eqs. (1) and (2)], and thus the basic assumption of our model, the comparison of the complicated spectra of the SD and DD detectors with the MD QDIPs underlines the supposition we already expressed in III: The vertical electron transport is heavily disturbed for the SD and DD devices due to a complete misalignment of the corresponding energy bands within the SL. Consequently, the photocurrent decreases by more than two orders of magnitude compared to the MD QDIPs.

Further, the model directly suggests that the strongest absorption for all devices should be found for the bound-to-bound ($S \rightarrow P_{\pm}$) transition. Therefore we performed PC measurements for MD-B, SD, and DD in the corresponding region around 60 meV as depicted in Fig. 8(b), together with the calculated absorption spectrum. In this case we have nearly perfect agreement between experiment and calculation. The observed photocurrent results from the optical excitation of electrons from the QD ground state into their first excited state. For the extraction of these electrons from the excited state into the SL miniband we suggest thermal ionization via highly excited QD or WL states. If further an unpolarized normal incidence geometry is chosen for the excitation, the shape anisotropy of the dots leaves its trace in the split-up of the main photocurrent peak. The PC measurement exhibits an energy separation of approximately 7 meV and a peak broadening of only 5 meV in all three devices, as predicted by our model for MD-B with slightly elliptic QDs. This means that despite the differences in the interband transitions and the PL linewidths of above 40 meV the intersublevel transition can be found at the same spectral position with a narrow linewidth for all three devices.

The double peak structure could also be confirmed by transmission experiments on a sample similar to the SD device.[40] However, it has to be noted that the currents in these PC experiments are very close to the lower detection limit of the measurement system, especially for the SD and DD devices. Only the strong decrease of the dark currents due to the AlAs barriers allows this small signal detection.

Because our model predicts a polarization dependence of the MIR absorption for the MD structures, we recorded the photocurrent of the ionization transition around 250 meV [see Fig. 8(a)] in dependence of the orientation of the incoming light field. Figure 9 shows the results for the QDIPs MD-B and MD-C for TM and TE polarizations. As sketched in this figure, TM corresponds in the chosen waveguide geometry mostly to a polarization parallel to z while TE can be regarded as normal incidence polarization. As expected from the model, the maximum signal is obtained for incoming light polarized parallel to the growth direction. Since a small part of the OS is left for the TE absorption (see the inset of Fig. 4), the PC signal does not drop to zero for this polarization. While the normalized photocurrent of MD-B agrees well with the model, device MD-C exhibits a much higher PC signal than expected for the polarization angle of 90° (i.e., TE-pol.). We attribute this deviation from the model to experimental problems like the smoothness of the backside of the waveguide, which leads to light scattering and the incoupling via parabolic mirrors that can cause deviations from the polarization angle set on the linear polarizer.

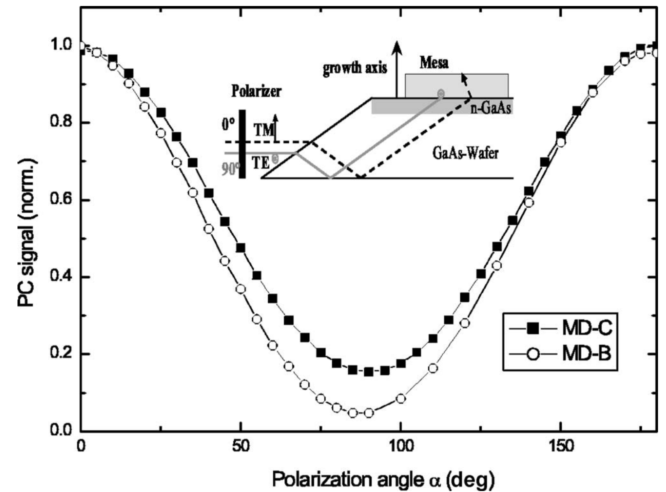

FIG. 9. Polarization dependence of the photocurrent peak maximum. The inset shows the waveguide structure of the device with corresponding polarization axes.

Summarizing our experimental results, we state that the combination of QD stacks and an AlAs/GaAs SL allows the design of very promising infrared detectors for the mid-infrared region. A comparison of our model with the experiments proves the suitability of our model for the design of QD-based photodetectors combined with AlAs/GaAs SLs: The energetic position of the absorption as well as the absorption peak widths were predicted correctly for all strictly periodic QD/SL devices. Further, we could deduce from the model the polarization properties of the detectors. QD stacks together with a SL structure strongly improve the SNR of our devices, but prefer clearly light polarizations along the growth axis of the detectors. A possibility to overcome this deficiency is given by our model: the $S \rightarrow P_{\pm}$ transition is a promising candidate for a new type of QDIP, where the excited states of the QDs will be energetically pushed into the quasicontinuum of the surrounding SL. First, measurements on this transition under normal incidence show a comparatively small photocurrent signal around 55 meV with a narrow linewidth. Due to the high absorption coefficient for these bound states and the strongly suppressed dark currents in the QD/SL devices, photoelectrons can be detected despite the fact that these structures were designed for the spectral region around 250 meV and do not allow a direct ionization with radiation around 55 meV. This shows the high potential of the periodic QD/SL detectors.

V. CONCLUSION

We investigated the suitability of combined QD/SL systems for the use as mid-infrared quantum dot photodetectors. Despite the fact that all devices are able to detect light in a normal incidence geometry, polarizations parallel to the growth direction cause the highest photocurrents for the chosen ionization transition. Our calculations show that this property cannot only be attributed to the SL, but also to the periodic arrangement of the QDs themselves. Comparing periodic QD/SL structures with nonperiodic QD arrangements

we could show that QDs together with their WL perturb the energetic structure of an AlAs/GaAs SL so heavily that both subsystems cannot be designed independently from each other. The model we developed for the periodic devices predicts not only the spectral response of the detectors, but also their polarization properties. Hence, our model allows designing the growth scheme for MIR QDIPs, and it further predicts a strong photocurrent under normal incidence, if QDs with bound ground states but excited states in the SL quasicontinuum are chosen. Further, we could show that vertical QD stacks within these SL structures should be preferred for the use as infrared photodetectors due to their higher spectral homogeneity, their high photocurrents, and low dark currents, as well as their possibility to design their spectral response by the surrounding SL.

ACKNOWLEDGMENTS

We would like to acknowledge the financial support by the Austrian Science Foundation FWF (SFB ADLIS, SFB IR-ON) and the European Community-IST projects ANSWER, SANDiE, and POISE. The LPA-ENS is "Laboratoire Associé au CNRS et aux Universités Paris 6 et Paris 7." Further, we would like to thank the Wolfgang Pauli Foundation (WPI Vienna) for their support.

---

*Corresponding author. Electronic address: schrey@tuwien.ac.at

†Present address: Nanoparc GmbH, Bautzner Landstraße 45, 01454 Dresden—Rossendorf, Germany.

‡Present address: Freescale Semiconductor, Crolles, France.

[1] L. Chu, A. Zrenner, G. Böhm, and G. Abstreiter, Appl. Phys. Lett. **75**, 3599 (1999).

[2] N. Horiguchi, T. Futatsugi, Y. Nakata, N. Yokoyama, T. Mankad, and P. M. Petroff, Jpn. J. Appl. Phys., Part 1 **38**, 2559 (1999).

[3] H. C. Liu, M. Gao, J. McCaffrey, Z. R. Wasilewski, and S. Farfard, Appl. Phys. Lett. **78**, 79 (2001).

[4] S. F. Tang, S. Y. Lin, and S. C. Lee, Appl. Phys. Lett. **78**, 2428 (2001).

[5] S. Hofer, H. Hirner, R. Bratschitsch, G. Strasser, and K. Unterrainer, Physica E (Amsterdam) **13**, 190 (2002).

[6] L. Rebohle, F. Schrey, S. Hofer, G. Strasser, and K. Unterrainer, Appl. Phys. Lett. **81**, 2079 (2002).

[7] S. Maimon, E. Finkman, G. Bahir, S. E. Schacham, J. M. Garcia, and P. M. Petroff, Appl. Phys. Lett. **73**, 2003 (1998).

[8] S. Sauvage, P. Boucaud, T. Brunhes, V. Immer, E. Finkman, and J. M. Gerard, Appl. Phys. Lett. **78**, 2327 (2001).

[9] Z. Ye, J. C. Campbell, Z. Chen, E. T. Kim, and A. Madhukar, J. Appl. Phys. **92**, 7462 (2002).

[10] L. Chu, M. Arzberger, G. Böhm, and G. Abstreiter, J. Appl. Phys. **85**, 2355 (1999).

[11] J. S. Kim, P. W. Yu, J. Y. Leem, M. Jeon, S. K. Noh, J. I. Lee, G. H. Kim, S. K. Kang, J. S. Kim, and S. G. Kim, J. Appl. Phys. **91**, 5055 (2002).

[12] K. W. Berryman, S. A. Lyon, and M. Segev, Appl. Phys. Lett. **70**, 1861 (1997).

[13] Z. Chen, E. T. Kim, and A. Madhukar, Appl. Phys. Lett. **80**, 2490 (2002).

[14] M. V. Maximov, A. F. Tsatsul'nikov, B. V. Volovik, D. A. Bedarev, A. Y. Egorov, A. E. Zhukov, A. R. Kovsh, N. A. Bert, V. M. Ustinov, P. S. Kop'ev, Z. I. Alferov, N. N. Ledentsov, D. Bimberg, I. P. Soshnikov, and P. Werner, Appl. Phys. Lett. **75**, 2347 (1999).

[15] J. Phillips, K. Kamath, and P. Bhattacharya, Appl. Phys. Lett. **72**, 2020 (1998).

[16] B. Aslan, H. C. Liu, M. Korkusinski, S.-J. Cheng, and P. Hawrylak, Appl. Phys. Lett. **82**, 630 (2003).

[17] E. Finkman, S. Maimon, V. Immer, G. Bahir, S. E. Schacham, F. Fossard, F. H. Julien, J. Brault, and M. Gendry, Phys. Rev. B **63**, 045323 (2001).

[18] E. T. Kim, A. Madhukar, Z. Ye, and J. C. Campbell, Appl. Phys. Lett. **84**, 3277 (1999).

[19] S. W. Lee, K. Hirakawa, and Y. Shimada, Appl. Phys. Lett. **75**, 1428 (1999).

[20] U. Bockelmann and G. Bastard, Phys. Rev. B **42**, 8947 (1990).

[21] J. Urayama, T. B. Norris, J. Singh, and P. Bhattacharya, Phys. Rev. Lett. **86**, 4930 (2001).

[22] A. Vasanelli, M. De Giorgi, R. Ferreira, R. Cingolani, and G. Bastard, Physica E (Amsterdam) **11**, 41 (2001).

[23] G. Fasching, K. Unterrainer, W. Brezna, J. Smoliner, and G. Strasser, Appl. Phys. Lett. **86**, 063111 (2005).

[24] O. Stier, *Electronic and Optical Properties of Quantum Dots and Wires*, Berlin Studies in Solid State Physics (Verlag Wissenschaft & Technik, Berlin, 2001).

[25] A. J. Williamson and A. Zunger, Phys. Rev. B **59**, 15819 (1999); **61**, 1978 (2000).

[26] A. Zunger, Phys. Status Solidi A **190**, 467 (2002).

[27] S. Lee, L. Jönsson, J. W. Wilkins, G. W. Bryant, and G. Klimeck, Phys. Rev. B **63**, 195318 (2001).

[28] P. Werner, K. Scheerschmidt, N. D. Zakharov, R. Hillebrand, M. Grundmann, and R. Schneider, Cryst. Res. Technol. **35**, 759 (2000).

[29] M. Fricke, A. Lorke, J. P. Kotthaus, K. Madeiros-Ribeiro, and P. M. Petroff, Europhys. Lett. **36**, 197 (1996).

[30] S. Hameau, Y. Guldner, O. Verzelen, R. Ferreira, G. Bastard, J. Zeman, A. Lemaitre, and J. M. Gerard, Phys. Rev. Lett. **83**, 4152 (1999).

[31] S. Hameau, J. N. Isaia, Y. Guldner, E. Deleporte, O. Verzelen, R. Ferreira, G. Bastard, J. Zeman, and J. M. Gerard, Phys. Rev. B **65**, 085316 (2002).

[32] D. P. Nguyen, N. Regnault, R. Ferreira, and G. Bastard, Phys. Rev. B **71**, 245329 (2005).

[33] P. Yu, W. Langbein, K. Leosson, J. M. Hvam, N. N. Ledentsov, D. Bimberg, V. M. Ustinov, A. Yu. Egorov, A. E. Zhukov, A. F. Tsatsul'nikov, and Yu. G. Musikhin, Phys. Rev. B **60**, 16680 (1999).

[34] G. Danan, B. Etienne, F. Mollot, R. Planel, A. M. Jean-Louis, F. Alexandre, B. Jusserand, G. Le Roux, J. Y. Marzin, H. Savary, and B. Sermage, Phys. Rev. B **35**, 6207 (1987).

[35] Source code available at http://www.phys.ens.fr/~reganult/diagham

[36] D. P. Nguyen, N. Regnault, R. Ferreira, and G. Bastard, Solid State Commun. **130**, 751 (2004).

[37] O. Stier, M. Grundmann, and D. Bimberg, Phys. Rev. B **59**, 5688 (1999).

[38] A. Vasanelli, R. Ferreira, H. Sakaki, and G. Bastard, Solid State Commun. **118**, 459 (2001).

[39] M. Tadic, F. M. Peeters, K. L. Janssens, M. Korkusinski, and P. Hawrylak, J. Appl. Phys. **92**, 5819 (2002).

[40] F. F. Schrey, T. Müller, G. Fasching, S. Anders, C. Pflügl, W. Schrenk, G. Strasser, and K. Unterrainer, Physica E (Amsterdam) **25**, 271 (2004).